Ionization balance in EBIT and tokamak plasmas

N. J. Peacock, R. Barnsley, M. G. O'Mullane, M. R. Tarbutt, D. Crosby et al.

Citation: Rev. Sci. Instrum. **72**, 1250 (2001); doi: 10.1063/1.1324755
View online: http://dx.doi.org/10.1063/1.1324755
View Table of Contents: http://rsi.aip.org/resource/1/RSINAK/v72/i1
Published by the American Institute of Physics.

Ionization balance in EBIT and tokamak plasmas

N. J. Peacock,[a] R. Barnsley,[b] and M. G. O'Mullane
Euratom/UKAEA Fusion Association, Culham Science Centre, Abingdon, Oxon OX14 3DB, United Kingdom

M. R. Tarbutt, D. Crosby, and J. D. Silver
The Clarendon Laboratory, University of Oxford, Parks Road, Oxford OX1 3PU, United Kingdom

J. A. Rainnie[c]
Department of Pure and Applied Physics, The Queen's University of Belfast, Belfast BT7 1NN, United Kingdom

(Presented on 22 June 2000)

The equilibrium state in tokamak core plasmas has been studied using the relative intensities of resonance x-ray lines, for example Ly_α (H-like), ''*w*'' (He-like), and ''*q*'' (Li-like) from test ions such as Ar^{+15}, Ar^{+16}, and Ar^{+17}. A full spatial analysis involves comparison of the line intensities with ion diffusion calculations, including relevant atomic rates. A zero-dimensional model using a global ion loss rate approximation has also been demonstrated by comparison with the data collected from a Johann configuration spectrometer with a charged coupled device (CCD) detector. Since the lines are nearly monoenergetic, their intensities are independent of the instrument sensitivity and are directly proportional to the ion abundances. This method has recently been applied to Ar in the Oxford electron beam ion trap (EBIT) with a beam energy in the range 3–10 keV. Taking into account the cross sections for monoenergetic electron collisions and polarization effects, model calculations agree with the observed line ratios at 4.1 keV beam energy. This work will be expanded to provide nomograms of ionization state versus line intensity ratios as a function of EBIT beam energy. [DOI: 10.1063/1.1324755]

I. INTRODUCTION

In this article, comparison of the x-ray emission spectra from highly ionized argon in the Joint European Torus (JET), tokamak with the same emission lines in an electron beam ion trap,[1–3] namely the Oxford EBIT,[4] indicates the relative ionization balance in these very different plasmas. It is argued that as in tokamaks the relative ion abundances in an EBIT are determined not only by atomic collision processes but also by a characteristic loss time τ_Z. The physical interpretation of this loss parameter depends on the operating conditions in these two plasmas.

Particle loss rates from tokamaks are often established through a study of the time and space dependence of the relative ion abundances of injected or intrinsic test ions. The concentrations of the ions are given by a solution of the coupled equations

$$\frac{\partial n_Z}{\partial t} = -\nabla.\Gamma_Z + n_e(n_{Z-1}S_{Z-1} - n_Z S_Z + n_{Z+1}\alpha_{Z+1} - n_Z\alpha_Z) - \frac{n_Z}{\tau_Z} + \gamma_Z,$$

where S and α are the appropriate ionization and recombination coefficients while τ and γ are the nondiffusive loss and influx terms, respectively. Given that the local flux of ions of charge state z, atomic number Z, is described by a diffusive (D) and convective (V) equation

$$\Gamma_Z = -D(r)\nabla n_Z(r) + V(r)n_Z(r),$$

then profiles of the D and V coefficients are selected that give computed emission profiles in agreement with the measured radial distribution of the ions.

It is the practice to measure a restricted range of line and continuum radiances and fit these data to an ion transport code such as SANCO[5] which can encompass a relevant atomic data base such as ADAS.[6,7] It is common to assign the convection term the form

$$V(r) = -2\frac{D(r)rS}{a^2},$$

where S is the dimensionless ''pinch'' parameter,[8] and $0 < S < 3$. Uncertainties in the transport and atomic physics modeling as well as errors in the absolute radiances make these detailed transport simulations a complex, lengthy, and often error-prone procedure. A simpler algorithm is to relate the ion balance, through intensities of resonance emission lines from successive ion charges, to a global ion confinement time, τ_Z,

$$\frac{\partial n_Z}{\partial dt} = -\frac{n_Z}{\tau_Z} + \gamma_Z + n_e(n_{Z-1}S_{Z-1} - n_Z S_Z + n_{Z+1}\alpha_{Z+1} - n_Z\alpha_Z),$$

where

[a]Electronic mail: nicol.peacock@ukaea.org.uk
[b]Attached to the Department of Physics, University of Leicester, LE1 7RH, UK.
[c]Present address: Euratom/UKAEA Fusion Association, Culham Science Center, Abingdon, Oxon, OX14 3DB, UK.

TABLE I. Argon emission lines analyzed in this work.

Ion	Label	λ (Å)
ArXVIII	Ly_{α_1}	3.7311
ArXVIII	Ly_{α_2}	3.7365
ArXVII	''w''	3.9490
ArXVII	''x''	3.9657
ArXVII	''y''	3.9693
ArXVII	''z''	3.9943
ArXVI	''q''	3.9810

$$D_Z=\frac{a^2}{(2.4^2-1.4S)\times\tau_Z}.$$

In a tokamak such as JET with the minor plasma radius ~1 m and with $0.05<D_Z<0.5\,\mathrm{m^2s^{-1}}$, depending on the confinement mode, τ_Z in the core plasma can vary between ~0.2 s and a few seconds. Thus $\tau_{eq}\sim 1/\alpha_Z$, the time to reach ionization-recombination balance, is $\tau_{eq}<\tau_Z$, and the relative ion abundance is only temperature T_e dependent. For smaller tokamaks like COMPASS the ionization balance in Cl has been demonstrated[9] to be τ_Z dependent in lossy plasmas with $\tau_{eq}>\tau_Z$.

The object of this article is to apply the same principles to an EBIT plasma where again ionization balance is of interest[10,11] and considerable effort has been expended on writing ionization balance codes.[12,13] In the present article we deal with a version of the ionization balance code termed OXGAS.[14] Analogously in the case of the EBIT we can define a loss τ_Z where

$$\frac{1}{\tau_Z}=\frac{1}{\tau_{esc}}+\frac{1}{\tau_{eq}},$$

and τ_{esc} is the escape time from the trap which depends on such factors as evaporative cooling[10] and gas flow, trap potential, and beam energy. However, τ_{eq} depends only on monoenergetic electron collision rates such as ionization, radiative recombination, and charge exchange with neutral thermal argon atoms. The highly charged ions are assumed to visit all regions in the EBIT trap. In the case of resonances between multiply excited levels and the beam energy, dielectronic recombination also has to be admitted. The argon emission features studied here are the $n=2\rightarrow 1$ resonance lines of Li-like, He-like, and H-like ions as indicated in Table I. The term diagram for the He-like ions and the Li-like ion satellites and their labels[15] are as indicated in Fig. 1.

II. ION ABUNDANCES FROM Ar SPECTRAL LINE EMISSION (MAXWELLIAN EXCITATION)

Except in the presence of non-Maxwellian electron beams[16] in tokamaks, magnetic confinement emission is isotropic and unpolarized. In the x-ray region, line splitting due to induced Lorentz electric fields and Zeeman splitting resulting from the main toroidal field is small relative to mass motion spectral shifts. The line radiance from a tokamak in terms of the volume emissivity ϵ_{ij} and then the ion abundance q_Z is given by

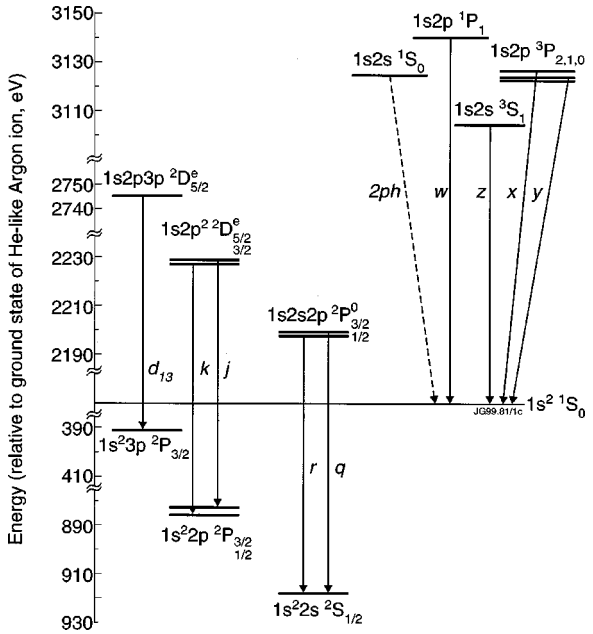

FIG. 1. Energy level diagram of $n=1\rightarrow 2$ transitions in ArXVI and ArXVII.

$$I_{ij}=\frac{\epsilon_{ij}}{4\pi}=n_e q_Z R_i\ \frac{A_{ij}}{\Sigma A_{ij}} h\nu_{ij},$$

where R_i, the relative excited state population, can be calculated using the ADAS population structure code.

Sample spectra of ArXVIII and ArXVII from the JET tokamak are indicated in Figs. 2 and 3, respectively. The relative abundances of argon ions [Fig. 4 (top)] and the associated line intensities [Fig. 4 (bottom)] in JET discharge #33311 are calculated using the SANCO ion transport code with the ADAS atomic physics package. The transport coefficients $D(r)$ and $V(r)$ shown in Fig. 4 have been derived previously by fitting to the transient spectral signature of injected test ions. The ratio of ''q/w'' assumes considerable

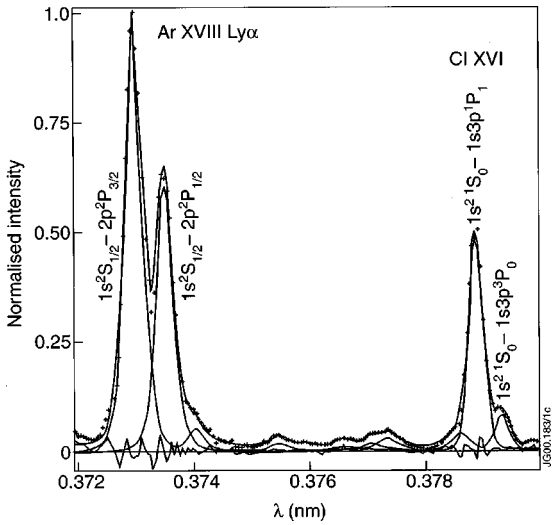

FIG. 2. JET spectrum of ArXVIII $Ly_{\alpha_{1,2}}$ using a Ge(111) double crystal spectrometer with collimation resulting in $\lambda/\Delta\lambda\approx 3500$.

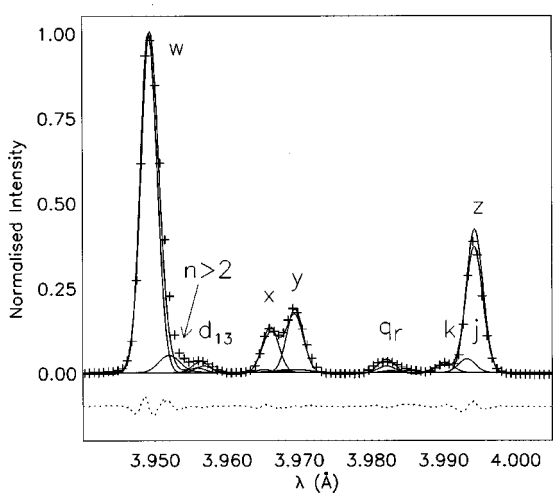

FIG. 3. JET (#49704) spectrum of ArXVII $n=1\rightarrow 2$ transitions and satellites using the CCD Johann spectrometer with a Si(111) crystal.

significance since the upper states of each line are populated directly from the ground states of adjacent ion charges, viz.

$$\frac{I_q}{I_w}=\frac{n(\mathrm{Ar}^{+15})}{n(\mathrm{Ar}^{+16})}\times\frac{\langle\sigma\nu\rangle_q}{\langle\sigma\nu\rangle_w}\times\frac{A_{qg}}{\Sigma_{r=1}^{\infty}A_{qr}+A_{qa}}.$$

The last factor, the transition rate branching ratio, which takes into account the ratio of A_{qg} to the total decay and Auger rates, is 0.942 for the I_q line.[17] In the temperature range $200\,\mathrm{eV}<T_e<20\,\mathrm{keV}$ the ratio of the excitation rates $\langle\sigma\nu\rangle_{q,w}\approx 1$ whether using *R*-matrix or the Born approximation. Thus $\langle\sigma\nu\rangle_{q,w}\approx f_{q,w}$ and an assumption of equal ion abundances gives $I_q/I_w\sim 1$. The ''q/w'' intensity ratio is directly a measure of $N(\mathrm{Ar}^{+15})/N(\mathrm{Ar}^{+16})$ and reaches a maximum of $\sim$15% at the outer edge of the normalized plasma radius. In the core with $T_e\sim 5\,\mathrm{keV}$, the ratio is $<10^{-3}$. In magnetically confined fusion plasmas the ''q/w'' and ''w/Ly_{α_1}'' intensity ratios, calculated as shown in Figs. 5 and 6, respectively, with ion confinement time as a parameter, are directly related to the ionization balance which in the steady state is determined by diffusive equilibrium. Since in JET with multi-keV temperatures τ_Z typically exceeds 0.1 s, then the ''q/w'' intensity ratio is always close to the coronal value.

III. EXPERIMENTAL METHOD AND DATA ANALYSES (BEAM EXCITATION)

In contrast to the tokamak plasma, emission from an EBIT is anisotropic[18] and polarized[19] about the monoenergetic beam direction. Considering for a moment the spatially integrated total line intensity I_{ij}, then

$$I_{ij}=\frac{j_e}{e}\sigma(\epsilon_{ij})N^{+Z},$$

where ϵ is the beam energy, j_e is the electron beam current density, and σ is the electron-impact excitation cross-section. The ratio of lines ''q/w,'' for example, is given by

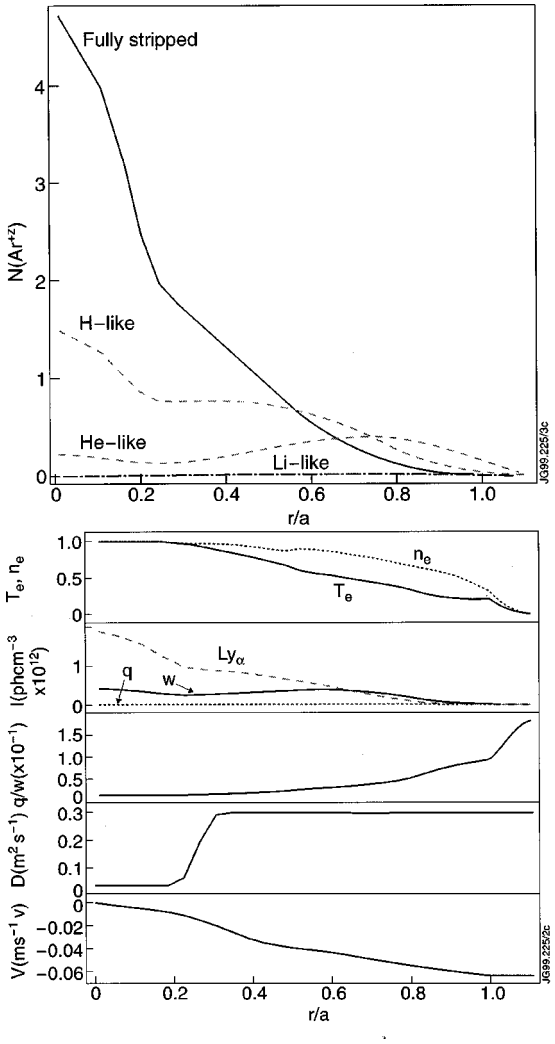

FIG. 4. Relative ion abundances (top) of argon ions and associated line intensities (bottom) in JET discharge #33311 at 57 s. $T_e(r/a=0)$ is 4.8 keV and $n_e(r/a=0)$ is $4.2\times 10^{-19}\,\mathrm{m}^{-3}$. The ion abundances are represented by the intensities of the resonance line $\mathrm{Ly}_\alpha(\mathrm{Ar}^{+17})$, ''w'' ($\mathrm{Ar}^{+16}$), and ''q'' ($\mathrm{Ar}^{+15}$) calculated by a diffusive equilibrium code (SANCO) with diffusive and convective transport coefficients as shown (bottom).

$$\frac{I_q}{I_w}=\frac{N(\mathrm{Ar}^{+15})}{N(\mathrm{Ar}^{+16})}\times\frac{\sigma(\epsilon)_q}{\sigma(\epsilon)_w}\times\frac{A_{qg}}{\Sigma_{r=1}^{\infty}A_{qr}+A_{qa}}.$$

Predictions using the OXGAS code for the Ar ion charge states in the Oxford EBIT with continuous gas feed are illustrated in Fig. 7 for an ion trap integration time of 3 s. At a beam energy of 4.1 keV,

$$\frac{I_q}{I_w}=\frac{N(\mathrm{Ar}^{+15})}{N(\mathrm{Ar}^{+16})}\times 1.31\times 0.932.$$

Assuming equal abundances of Ar^{+15} and Ar^{+16} the ''q/w'' intensity ratio would therefore be 1.23. The experimental derivation of ion abundances from these lines requires a serious consideration of the spatial variation of the intensity and polarization[20,21] of the different transitions due to the monodirectional beam excitation. In addition the crystal diffraction is polarization dependent.[22] The observed line intensity is then $I_{\mathrm{OBS}}=R_\parallel I_\parallel+R_\perp I_\perp$, where R is the crystal reflectivity and $I_\parallel$, $I_\perp$ are the intensities of the polarizations parallel and othogonal to the beam, respectively. Generally,

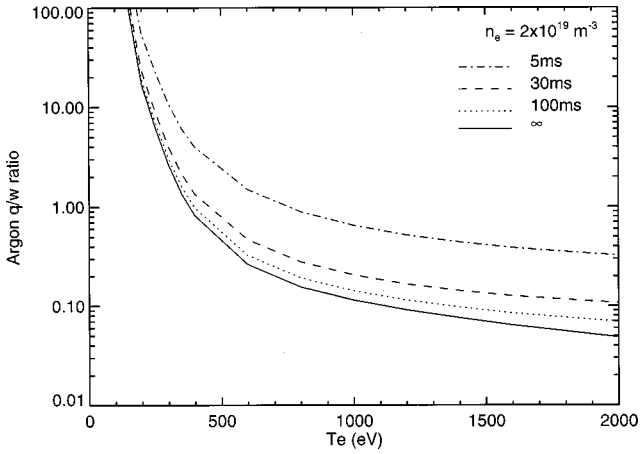

FIG. 5. Calculated intensity ratio of ''*q*'' (Li-like)/''*w*'' (He-like) emission lines from argon as a function of T_e with τ_Z as a parameter.

$R = R_\perp / R_\parallel = \cos^m 2\theta$ with $1 < m < 2$. In order to calculate the effects of anistropy and polarization we need to consider in some detail the experimental setup.

The variable geometry, Johann configuration x-ray spectrometer with CCD read-out[23] has previously been used[9,24] to study emission spectra from the JET and COMPASS tokamaks. The CCD spectrometer with its capability for long signal integration times and low noise is in fact even more ideally suited to the present application of the study of the EBIT. In the Johann geometry where the crystal radius is the diameter of the Roland circle ($R_C = 2r$), the waveband, sensitivity, and resolving power are interdependent and depend on the spatial dimensions of the source. For extended sources such as tokamaks the $F/no.$, i.e., w/R, is equally filled for a range of wavelengths satisfying the Bragg condition. In contrast, the EBIT ''point source'' was arranged in the present experiments to be within the Rowland circle as indicated in Fig. 8, in order to achieve a finite bandwidth, albeit at the expense of sensitivity. The dispersion plane is orthogonal to the axis of the EBIT.

The angular bandwidth is then $\Delta\Phi = (w \sin\theta/b) - (w/R) + (x/b)$ where w is the crystal width, x is the source width, θ is the Bragg angle, and b is the distance between the source and the pole of the curved diffractor Si(111). For the $Ar^{+17,+16}$ spectra shown, $w \approx 25$ mm, $R = 1394$ mm, (x/b) is negligible, and $\Delta\theta \approx 3 \times 10^{-3}$. Thus the bandwidth $\Delta\lambda \approx 20$ mÅ, which in contrast to the tokamak viewing geometry is insufficient to cover the whole $n = 2 - 1$ emission spectrum from Ar^{+16}. The spectrum shown in Fig. 9 is a composite $\Delta\lambda_{COM} = \Delta\lambda_1 + \Delta\lambda_2 + \Delta\lambda_3$, where $\Delta\lambda_{1,2,3}$ are exposures at different source positions and diffraction from different, local ($\sim$1 mm) regions of the crystal curvature. This will affect somewhat the relative line intensities. The resolving power of the spectrometer $\lambda/\Delta\lambda \approx 3500$ as can be seen from the well-separated components of $Ly_{\alpha_1} - Ly_{\alpha_2} = 5.5$ mÅ in Fig. 10.

Introducing the polarization factor $P = (I_\parallel - I_\perp)/(I_\parallel + I_\perp)$, where $I_\parallel + I_\perp = I(90°)$ and where the intensity[18] viewed orthogonal to the beam $I(90°) = 3I/(3-P)$, then the relative intensities of two different lines from the same ion species are given by

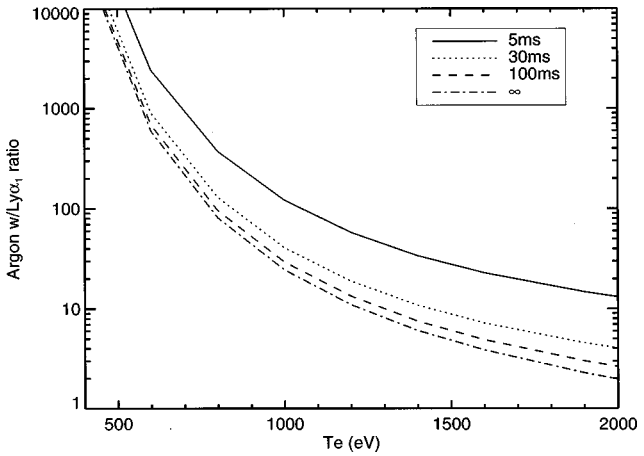

FIG. 6. Calculated intensity ratio of ''w'' (He-like)/Ly_{α_1} (H-like) emission lines from argon as a function of T_e with τ_Z as a parameter.

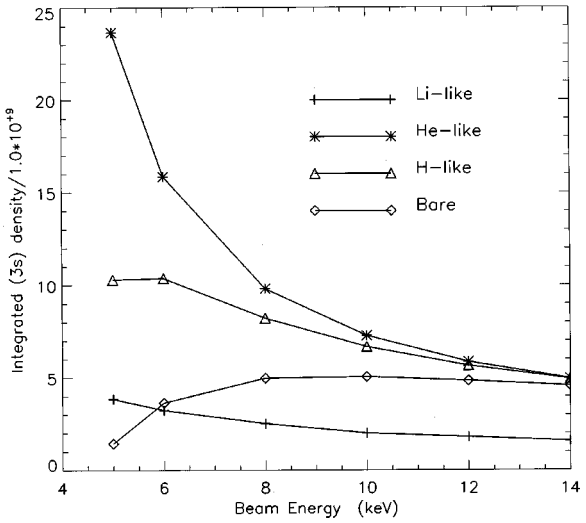

FIG. 7. OXGAS predictions of the relative abundance of argon ions as a function of beam energy for $B = 2.7$ T, $j_e = 50$ mA and $N(\mathrm{Ar}) \approx 10^5$ cm^{-3}. The gas feed rate is continuous and the counts integrated over a 3 s period.

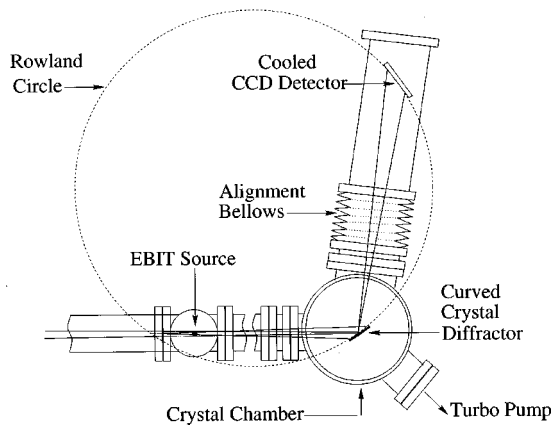

FIG. 8. Optical layout of the CCD spectrometer on the EBIT source.

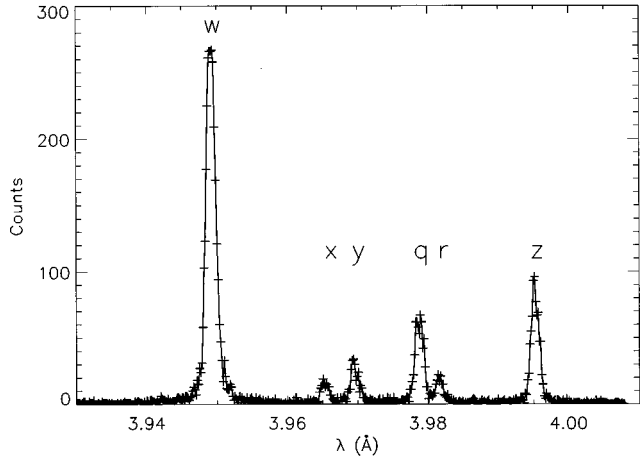

FIG. 9. EBIT spectrum of $n=2\rightarrow1$ transitions in ArXVII and ArXVI at $\epsilon_b=7.0$ keV.

$$\frac{I_a}{I_b}=\frac{(1+P_a)+R(1-P_a)}{(1+P_b)+R(1-P_b)}\times\frac{3-P_b}{3-P_a}\times\frac{\sigma_a}{\sigma_b}.$$

The first factor on the rhs accounts for the different crystal reflectivities[25] to the $\perp$ and $\parallel$ components while the second factor is the fraction of $I(90°)$ to the total emission.

Inserting the total cross sections for excitation by electron impact for the He-like ArXVII $n=2-1$ lines and adopting the polarization parameters suggested by Beiersdorfer *et al.*,[21] the calculated relative intensities for ''*w*,'' ''*x*,'' ''*y*,'' and ''*z*'' in the orthogonal plane are as indicated in Fig. 11. Assuming a crystal reflectivity[25] $R=0.201$, then the calculated relative intensities after diffraction are also shown and can be compared with the data in Fig. 9. The effect of polarization in the adopted geometry is to substantially suppress the triplet ''*x*'' and ''*y*'' lines. The observed ''*z*'' intensity and the important Ar^{+15}/Ar^{+16} charge state indicator ratio ''*q*''/''*w*'' are less affected. Applying the same analysis to the ''*q*''/''*w*'' intensity ratio, we have

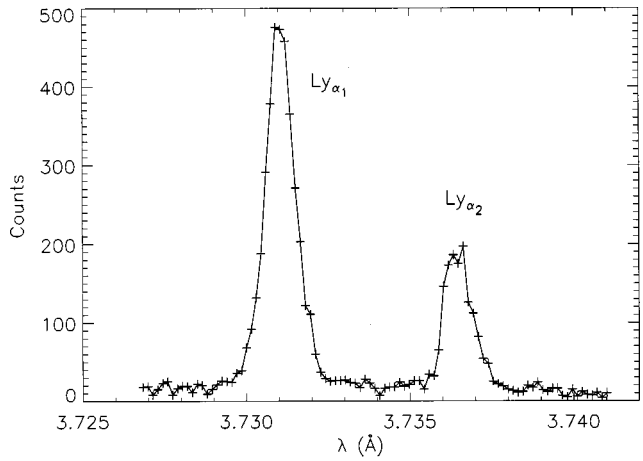

FIG. 10. EBIT spectrum of Ar $Ly_{\alpha_{1,2}}$ at $\epsilon_b=7.0$ keV.

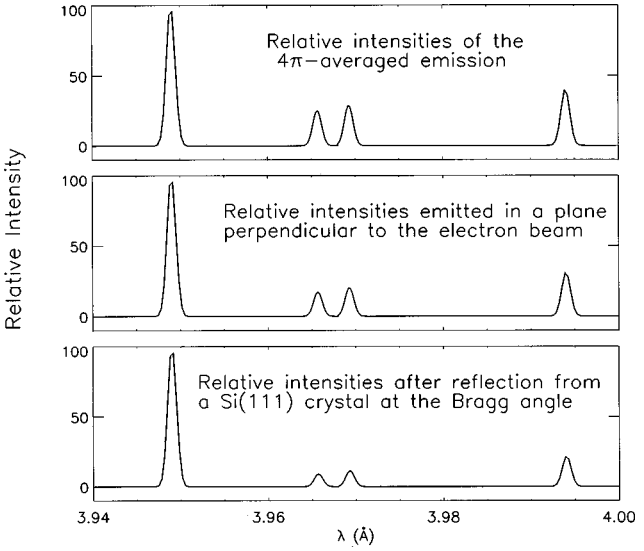

FIG. 11. Calculated relative intensities of the $n=1\rightarrow2$ transitions in ArXVII from an EBIT with $\epsilon_b=4.1$ keV. The effects of emission anisotropy on the viewing angle and on reflection from the Si(111) crystal are shown.

$$\frac{I_q}{I_w}=\frac{N(Ar^{+15})}{N(Ar^{+16})}\times1.31\times0.932\times\frac{(1+P_q)+R(1-P_q)}{(1+P_w)+R(1-P_w)}\times\frac{3-P_w}{3-P_q}.$$

Inserting values for $P_w=0.6$, $P_q=0.33$, and $R=0.201$, then

$$\frac{I_q}{I_w}=0.957\times\frac{N(Ar^{+15})}{N(Ar^{+16})}.$$

Predictions of the OXGAS code[14] for the appropriate operating conditions of $\epsilon_b=4.1$ keV, trap potential=400 V, $B=2.7$ T, $j_e=50$ mA, and 3 s integration time with continuous Ar gas feed gives values of $N(Ar^{+15})/N(Ar^{+16})$ between 0.17 and 0.19 for a neutral Ar density parameter of 1×10^3 and 4×10^5 cm^{-3}. The code is therefore in excellent

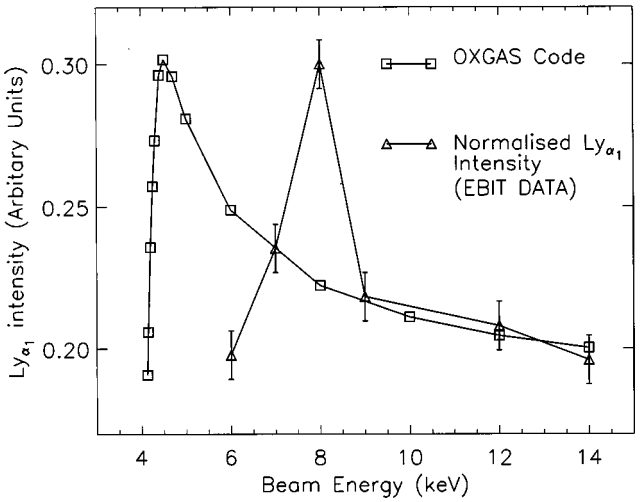

FIG. 12. Intensity of ArXVIII Ly_{α_1} as a function of beam energy compared to OXGAS predictions with $B=2.7$ T, $j_e=100$ mA, $N(Ar)\approx10^5$ cm^{-3}, and $V_T=400$ eV.

agreement with the experimental ratio of 0.2. At higher beam energies, above 5 keV, the code seems to overestimate the degree of ionization in the trap. This can be appreciated by comparing the montonically decreasing ArXVIII ion abundance with beam energy predicted by the code with the measured intensity of ArXVIII Ly_α (Fig. 12). The experimental data shows, in contrast, a maximum at about $\epsilon_b = 8$ keV.

An attempt has been made to relate the ion abundances in EBIT to a global loss term in the same manner as for tokamak plasmas. However, in tokamaks the neutral fuel influx and the electron density are related. The situation in the EBIT is more complex since here n_e and $N(\mathrm{Ar}^0)$ have to be separately specified. We choose the related parameters of $N(\mathrm{Ar}^0)/j_e = \mathcal{R}$ as a ratio parameter which describes a 3-D surface with ion abundance and beam energy. Figure 13 illustrates such a calculation for specific values of the EBIT operational parameters.

IV. SUMMARY

The use of appropriate ion abundance codes for predicting the relative intensities of the main $n=2\rightarrow1$ resonance lines in H-, He-, and Li-like ions of argon in Maxwellian and beam-excited plasmas appears to be justified. With a core temperature, $T_e(r/a=0) \ll 1$ keV in a tokamak, ''q/w'' can be of the same order as observed in the EBIT with a beam energy of 4.1 keV, ionization-recombination equilibrium being a good approximation for well-confined plasmas in both sources. In tokamaks, the concept of a global loss rate has applications to the diagnostic use of the relative resonance line intensities to determine diffusive equilibrium coefficients. In an EBIT plasma the model is less readily applicable and requires multidimensional parameter fitting. Global loss rates may be so low relative to the source influx term that ion abundance equilibrium is never reached. In the opposite situation where the trap is leaky with a leak rate on the same time scale as the ionization rates, then the calculated nomograms of relative line intensities versus beam energy may be useful in establishing the actual mechanisms of the loss processes.

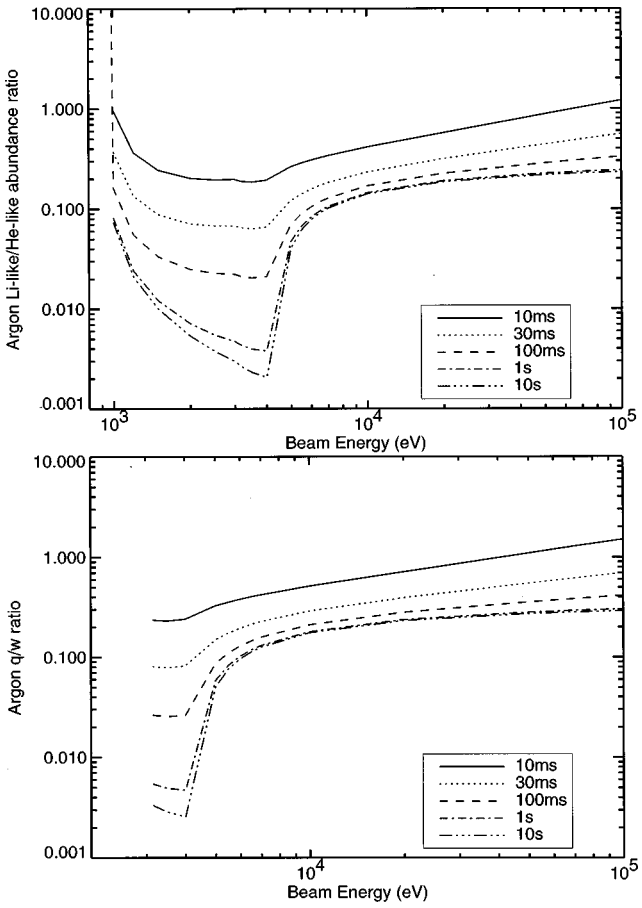

FIG. 13. Global loss model of $N(\mathrm{Ar}^{+15})/N(\mathrm{Ar}^{+16})$, the relative ion abundances (top) and ''q'' (Li-like)/''w'' (He-like), and the relative line intensities (bottom) in an EBIT trap as a function of beam energy with the loss time as a parameter. $N(\mathrm{Ar}^0)=1\times10^5\ \mathrm{cm}^{-2}$, $j_e=4.2\times10^3\ \mathrm{A/cm}^{-2}$, and $T_i=1.0$ keV.

ACKNOWLEDGMENTS

M.G.O'M. was supported through an ADAS contract, Department of Physics and Applied Physics, University of Strathclyde, Glasgow, G4 0NG, UK. This work is partly funded by the UK Department of Trade and Industry and EURATOM. The diagnostic development has been supported by UKAEA-Fusion.

[1] M. A. Levine, R. E. Marrs, J. R. Henderson, D. A. Knapp, and M. B. Schneider, Phys. Scr., T **T22**, 157 (1998).
[2] M. A. Levine *et al.*, Nucl. Instrum. Methods Phys. Res. B **43**, 431 (1989).
[3] R. Schmieder, *Physics of Highly Ionised Atoms*, Vol. 201 of ASI Nato Series, edited by R. Marrus (Plenum, New York, 1989), p. 321.
[4] J. D. Silver *et al.*, Rev. Sci. Instrum. **65**, 1072 (1994).
[5] L. Lauro-Taroni (private communication, JET, 1994). See also L. Lauro-Taroni *et al.*, Proc. 21st EPS Conference on Controlled Fusion and Plasma Physics, Montpellier, published in Europhysics Conference Abstracts (1994), Vol. 1, p. 102.
[6] H. P. Summers, *Atomic Data and Analysis Structure. User Manual JET-IR 94(06)*, 1994.
[7] H. P. Summers and M. von Hellerman, *Atomic and Plasma-Material Interaction Processes in Controlled Thermonuclear Fusion*, edited by R. K. Janev and H. W. Drawin (Elsevier Science, Amsterdam, 1993), pp. 87–117.
[8] F. H. Seguin, R. Petrasso, and E. S. Marmar, Phys. Rev. Lett. **51**, 455 (1983).
[9] I. M. Melnick, Ph.D. thesis, University College London, 1995.
[10] R. W. Schmieder, Phys. Scr., T **T22**, 312 (1988).
[11] F. Decaux, P. Beiersdorfer, S. M. Khan, and V. L. Jacobs, Astrophys. J. **482**, 1076 (1997).
[12] B. M. Penetrante, J. N. Bardsley, D. DeWitt, M. Clark, and D. Schneider, Phys. Rev. A **43**, 4861 (1991).
[13] B. M. Penetrante, J. N. Bardsley, M. A. Levine, D. A. Knapp, and R. E. Marrs, Phys. Rev. A **43**, 4873 (1991).
[14] H. Margolis, Ph.D. thesis, University of Oxford, 1994.
[15] A. H. Gabriel, Mon. Not. R. Astron. Soc. **160**, 99 (1972).
[16] M. K. Inal and J. Dubau, J. Phys. B **20**, 4221 (1987).
[17] M. S. Chen, At. Data Nucl. Data Tables **34**, 301 (1986).
[18] I. C. Percival and M. J. Seaton, Philos. Trans. R. Soc. London, Ser. A **251**, 113 (1958).
[19] M. K. Inal and J. Dubau, Phys. Rev. A **47**, 4794 (1993).
[20] P. Beiersdorfer *et al.*, Phys. Rev. A **53**, 3974 (1996).
[21] P. Beiersdorfer, J. Crespo López-Urrutia, V. Decaux, K. Widmann, and P. Neill, Rev. Sci. Instrum. **68**, 1073 (1997).
[22] A. Burek, Space Sci. Instrum. **2**, 53 (1976).
[23] A. F. Abbey, R. Barnsley, J. Dunn, S. N. Lea, and N. J. Peacock, *UV and X-Ray Spectroscopy of Laboratory and Astrophysical Plasmas* (Cambridge University Press, Cambridge, 1993), p. 493.
[24] I. V. Coffey, Ph.D. thesis, The Queen's University of Belfast, 1993.
[25] B. L. Henke, E. M. Gullikson, and J. C. Davis, At. Data Nucl. Data Tables **54**, 181 (1993).